Computers & Fluids Vol. 16, No. 3, pp. 257–278, 1988
Printed in Great Britain.

0045-7930/88 $3.00 + 0.00

AN EXAMINATION OF FORCING IN DIRECT NUMERICAL SIMULATIONS OF TURBULENCE

V. ESWARAN and S. B. POPE

Sibley School of Mechanical and Aerospace Engineering, Cornell University, Ithaca, NY 14853, U.S.A.

(*Received* 15 *June* 1987; *in revised form* 2 *November* 1987)

Abstract—A spectral forcing scheme is developed to provide the means to obtain statistically stationary velocity fields in direct numerical simulations of homogeneous, isotropic turbulence. Tests of the forcing scheme show that the details of the forcing do not have a significant effect on the small-scale structure of the velocity fields.

Forced turbulent simulations are used to determine the effects of the time-step, and the spatial resolution of the grid, on the computations.

INTRODUCTION

A tenet of much turbulence research is that the small-scale behavior of turbulent velocity fields is universal. That is, the small-scale structure of a wide variety of turbulent flows is similar, depending only (and weakly) on the Reynolds number. This universality gives any study of such small-scale structure general applicability. However, our current knowledge of this area is limited due to practical constraints on experimental studies of turbulent flows.

In the last 15 years, improvements in the power of computers have enabled researchers to use highly accurate techniques to solve the Navier–Stokes equations numerically (using no modelling) in order to obtain the transient velocity fields of moderate-Reynolds-number flows. Such simulations have demonstrated the capability of reproducing experimentally-obtained data for many flows (see, e.g. Ref. [1]). Therefore, a study of small-scale behavior using direct numerical simulations (DNS) has a sound physical basis. A number of researchers have already attempted such studies (e.g. Siggia and Patterson [2]; Siggia [3]; Kerr [4]).

Direct numerical simulations of isotropic flows using pseudo-spectral methods began with the work of Orszag and Patterson [5]. Since then the techniques have been extended to anisotropic homogeneous flows (e.g. Ref. [6]) and to inhomogeneous flows (e.g. Ref. [7]). The methods generally involve transformation of the velocity field into a sum of eigenfunctions in spectral space (e.g. by discrete Fourier transforms) and the numerical solution of the Navier–Stokes equations in spectral form. Compared to finite-difference methods, such a procedure enhances the accuracy of the evaluation of the spatial derivatives that appear in the Navier–Stokes equations [8, 9]. Reviews of the published work in this field have been provided by Rogallo and Moin [1] and Hussaini and Zang [10].

Small-scale behaviour in turbulent flows tends to be characterized by statistical homogeneity, isotropy and universality. Because of this universality we can hope to understand small-scale behavior by studying the simplest turbulent flows, i.e. homogeneous, isotropic turbulence. However, homogeneous, isotropic turbulence is not statistically stationary. Stationary turbulence lends itself more easily to statistical analysis, especially if multi-time statistics are required as in the work of Yeung and Pope [11], for example.

One way to generate a statistically stationary velocity field is to "force" the low-wavenumber (i.e. large scale) velocity components in the simulation by artificially adding energy. This energy cascades to the small scales and is dissipated by viscous action. Starting from an (almost) arbitrary initial condition, a statistically stationary state is achieved after some time, in which the average rate of energy addition to the velocity field is equal to the average energy-dissipation rate.

Forcing is by no means a new idea. Siggia and Patterson [2], Siggia [3] and Kerr [4] used forcing schemes in numerical investigations of small-scale structure.

Although certain small-scale quantities (the energy-dissipation, for example) are essentially determined by the large-scale dynamics, it is generally accepted that the dynamics of the small-scales are decoupled from the details of the large-scale behaviour, in high-Reynolds-number turbulent flows (see e.g. Ref. [12]). The assumption inherent in the use of low-wavenumber forcing is that the time-averaged small-scale quantities will not be influenced by the details of the mechanism for energy-production at the large scales but will depend, rather, on its gross effects, i.e. the energy-production rate, the kinetic energy, etc. This is closest to the truth, however, when the smallest and the largest scales are widely separated, i.e. when the Reynolds number is high. Then Kolmogorov's hypotheses [13] support the assumption. These hypotheses are even more restrictive than the forcing assumption, assuming—as they do—that, at high enough Reynolds numbers, the large scales influence the small-scale statistics only to the extent of determining the energy-dissipation. DNS, however, can be used to simulate only moderate-Reynolds-number turbulence. It is, therefore, necessary to show that forcing can justifiably be used in DNS. For the forcing assumption to be good, it is necessary that the computed high-wavenumber quantities do not depend on the details of the forcing scheme.

A systematic study of the use of forcing has not previously been published. We present a new forcing scheme that avoids some of the disadvantages of the previous schemes. We report numerical tests to demonstrate that the small-scale statistics are insensitive to the details of the forcing. We have also parametrized the important flow quantities, like the Reynolds number, in terms of the forcing variables. This enables one to chose, *a priori*, the forcing parameters for a flow-simulation of a desired Reynolds number.

We have also explored three issues of importance, which have not yet been studied systematically in the published literature:

First, the effect of the Courant number on the computations has been investigated. The Courant number is the normalized time-step used in the simulations; higher Courant numbers yield larger time-steps, thereby decreasing the overall computer time. However, if the Courant number is too large, the truncation errors become unacceptably large and instabilities can occur. Our computations confirm the general rule for explicit schemes that the Courant number should be less than unity.

Second, we examined the effect of spatial resolution on the high-wavenumber quantities. Turbulent velocity fields contain a range of length scales, the extent of which is determined by the Reynolds number. That is, the higher the Reynolds number, the greater is the ratio of the largest scales to the smallest scales present in the flow. The computational domain has to be large enough to resolve fully the range of length scales in the field. If the Reynolds number is increased beyond acceptable limits one would expect the quality of the simulations to degenerate. We examined this degradation with reference to the high-wavenumber quantities under consideration.

Third, we examined the effects of the anisotropy of the grid and the forcing upon the statistically stationary velocity field and conclude that they are not significant. That is, the computed velocity fields do not exhibit gross anisotropy.

In the next section we describe, briefly, the numerical method and the forcing scheme used in this study. The third section contains a brief overview of the prescribed and the derived parameters in the simulations, and of the high-wavenumber quantities considered. In the fourth section, the results of the simulations are presented.

THE NUMERICAL METHOD AND FORCING SCHEME

(a) The numerical method

The computer code used for this work is a version of the one developed by Rogallo [6]. It uses a pseudo-spectral method to solve the Navier–Stokes equations for incompressible flows on a 3-D uniform mesh. The time-stepping is performed by an explicit second-order

Runge–Kutta scheme. The viscous terms are treated exactly and are thus eliminated as a stability constraint.

In physical space, the solution domain is a cube of side L with N^3 grid points. The grid points are located at $\underline{x}$, where $\underline{x}$ is defined as $(l_1\Delta x, l_2\Delta y, l_3\Delta z)$ and l_1, l_2, l_3, are integers between 0 and $N-1$, inclusive. (For this study, $\Delta x = \Delta y = \Delta z = L/N$.) In wavenumber space there are N^3 discrete wavenumbers, $(m_1 k_0, m_2 k_0, m_3 k_0)$, where m_1, m_2, m_3, are integers between $1 - N/2$ and $N/2$, both inclusive. The lowest wavenumber, k_0, is equal to $2\pi/L$. The independent variables in the simulations are complex Fourier amplitudes of the velocity at these discrete wavenumbers, $\underline{k}$.

Let $\underline{u}(\underline{x}, t)$ be the velocity at the grid point, $\underline{x} = (l_1\Delta x, l_2\Delta y, l_3\Delta z)$. Then the corresponding Fourier coefficient, $\tilde{\underline{u}}(\underline{k}, t)$, at wavenumber $\underline{k}$, is given by:

$$\tilde{\underline{u}}(\underline{k}, t) = \frac{1}{N^3}\sum_{l_1}\sum_{l_2}\sum_{l_3}\underline{u}(\underline{x}, t)\exp(-i\underline{k}\cdot\underline{x}), \tag{1}$$

where the summation is over all grid nodes in physical space. The inverse-Fourier relationship is:

$$\underline{u}(\underline{x}, t) = \sum_{m_1}\sum_{m_2}\sum_{m_3}\tilde{\underline{u}}(\underline{k}, t)\exp(i\underline{k}\cdot\underline{x}), \tag{2}$$

where the summation is over all wavenumbers in wave-space. The boundary-conditions are periodic, i.e.:

$$\underline{u}(\underline{x} + \underline{n}L, t) = \underline{u}(\underline{x}, t), \tag{3}$$

where $\underline{n}$ is any integer vector. The mean velocity is assumed to be zero (from which it follows that $\tilde{\underline{u}}(0, t) = 0$).

The continuity and the Navier–Stokes equations can be written in wavenumber space as:

$$\underline{k}\cdot\tilde{\underline{u}}(\underline{k}, t) = 0, \tag{4}$$

and

$$\frac{\partial\tilde{\underline{u}}(\underline{k}, t)}{\partial t} = \tilde{\underline{a}}(\underline{k}, t), \tag{5}$$

where $\tilde{\underline{a}}(\underline{k}, t)$ is the Fourier coefficient of the rate of change of velocity with time, evaluated using the Navier–Stokes equations. The explicit expression for $\tilde{\underline{a}}(\underline{k}, t)$ can be found in Ref. [6].

The right-hand side of eqn (5) contains terms which are products of the velocity and its spatial derivatives. (The pressure term is expressed in terms of the velocity and its derivatives.) The spatial derivatives are evaluated in wavenumber space. To facilitate computation, the products are calculated in physical space. This last introduces aliasing errors which are virtually eliminated by a technique described below. Such a mixture of spectral and physical computations is generally labeled "pseudo-spectral".

For good resolution, the highest wavenumbers in the computational box must be sufficiently large to capture the smallest scales of the flow (characterized by the Kolmogorov length-scale, η). The highest significant wavenumber is determined, in part, by the method used to remove aliasing errors. The method used is a combination of truncation and phase-shifting (see Ref. [6]). As a result the physically significant wavenumbers in our computational scheme lie inside a sphere of radius, $k_{\max} = \sqrt{2}k_0 N/3$. An additional constraint on the simulations is that the integral length-scales of the velocity field must be sufficiently small, compared to L, to justify the use of periodic boundary conditions. In our simulations the integral length-scale (to be defined later) did not exceed $0.3L$. The value of N limits the ratio of the largest length scales to the smallest (and thereby the Reynolds number) of the simulations.

The time-advancement scheme is explicit. A Courant number restriction, determining the largest permissible time-step, is usual in explicit schemes. This limit is usually obtained from considerations of numerical stability rather than those of time-stepping errors. Knowledge of stability constraints in spectral algorithms is limited (see e.g. Ref. [14]) and no theoretically-obtained stability constraint is known for our scheme. However, a Courant number specification is a useful way to determine the time-step. In our case the Courant number, C, is defined as:

$$C = \left[\frac{|u|}{\Delta x} + \frac{|v|}{\Delta y} + \frac{|w|}{\Delta z}\right]_{\max} \Delta t, \tag{6}$$

where u, v, and w are the three components of velocity (in physical space) at a grid point, and Δt is the time-step.

With second-order Runge–Kutta time-stepping, the solution of eqn (5) requires that $\tilde{a}(\underline{k}, t)$ be evaluated twice per time-step. Therefore the velocity and other required fields are (discrete) Fourier-transformed four times (twice forward, twice inverse) per time-step. The computations are quite time-consuming. The demands on the computer's storage space are also non-trivial. Progress towards higher values of N and Reynolds numbers is effectively dictated by the power of the computer used. For $(64)^3$ calculations (i.e. $N = 64$), an FPS 264 array processor takes about 27 CPU seconds per time-step and typically takes about 18 CPU h to run a reasonably long simulation (2400 steps). The memory requirement is about eight Megabytes. Comparable $(128)^3$ simulations would require about 8 times that much storage and take about 300 CPU h.

(b) The forcing scheme

It has already been mentioned that Siggia and Patterson [2], Siggia [3], and Kerr [3] have used forcing to obtain statistically stationary velocity fields. Siggia and Patterson "froze" the velocity Fourier amplitudes in a low-wavenumber band to obtain statistical stationarity. Siggia used low wavenumber modes (which were not included in the spectral Navier–Stokes equations computational box) to force the simulations by modelling the rate-of-strain of the larger scales. Kerr time-stepped the modes in a low-wavenumber band conservatively according to the Euler equations. The energy in the band was thus kept constant.

All the forcing schemes mentioned above are successful in some respects, but they also have some defects. The "frozen-amplitude" method freezes the anisotropy in the large scales, so isotropic statistics can be obtained only by averaging over many computations. Simulations using the rate-of-strain-modelling method yield large fluctuations in the large-scale quantities (i.e. energy, dissipation rate, etc.) that are correlated over very large periods of time. This increases the time for which the simulations have to be performed to get time-averaged quantities with reasonably small statistical errors. The Euler-forcing technique preserves the helicity in the large scales which may have an unnatural effect on the turbulence.

In our scheme, the forcing is performed by adding a forcing acceleration, $\tilde{a}^F(\underline{k}, t)$ to $\tilde{a}(\underline{k}, t)$, in eqn (5), in a low-wavenumber band. This treatment is applied to all nodes within a sphere of radius K_F centered at the orign (but excluding the node at the origin). We have considered two cases with K_F equal to $\sqrt{2}k_0$ and $2\sqrt{2}k_0$, respectively. The number of nodes in the forced band, N_F, in these two cases are 18 and 92, respectively. Therefore, the equation determining the forced velocity field is:

$$\frac{\partial \tilde{u}(\underline{k}, t)}{\partial t} = \tilde{a}(\underline{k}, t) + \tilde{a}^F(\underline{k}, t), \tag{7}$$

where $\tilde{a}^F(\underline{k}, t)$ is non-zero only for wavenumbers, $\underline{k}$, that satisfy $0 < |\underline{k}| \leq K_F$.

The specification of the forcing acceleration $\tilde{a}^F(\underline{k}, t)$ is based on Uhlenbeck–Ornstein (UO) random processes (see, e.g. Ref. [15]). At each forced wavenumber we combine 6 independent UO processes, each with variance σ^2 and time-scale T_L, to form a complex vector-valued stochastic process denoted by $\tilde{b}(\underline{k}, t)$. This process is characterized by the

following properties:

$$\langle \tilde{\underline{b}}(\underline{k}, t)\rangle = 0, \tag{8}$$

and

$$\langle \tilde{b}_i(\underline{k}, t)\tilde{b}_j^*(\underline{k}, t+s)\rangle = 2\sigma^2 \delta_{ij} \exp(-s/T_L), \tag{9}$$

where, here and below, an asterisk denotes a complex conjugate, angle brackets indicate ensemble averages, and δ_{ij} is the Kronecker delta. In order to guarantee the required (continuity) condition $\underline{k}\cdot\tilde{\underline{a}}^F(\underline{k}, t) = 0$ (cf. eqn 4), we take $\tilde{\underline{a}}^F(\underline{k}, t)$ to be the projection of $\tilde{\underline{b}}(\underline{k}, t)$ onto the plane normal to $\underline{k}$:

$$\tilde{\underline{a}}^F(\underline{k}, t) \equiv \tilde{\underline{b}}(\underline{k}, t) - \underline{k}\,\underline{k}\cdot\tilde{\underline{b}}(\underline{k}, t)/(\underline{k}\cdot\underline{k}). \tag{10}$$

Through this forcing scheme, three positive parameters are introduced: the amplitude σ, the time-scale T_L, and the maximum wavenumber of the forced modes, K_F. It is simply deduced from eqn (7) that the rate of energy addition, $\dot{E}_F$, due to forcing is:

$$\dot{E}_F = \tfrac{1}{2}\Sigma_{m_1}\Sigma_{m_2}\Sigma_{m_3}\{\langle \tilde{\underline{a}}^F(\underline{k}, t)\cdot\tilde{\underline{u}}^*(\underline{k}, t)\rangle + \langle \tilde{\underline{a}}^{F*}(\underline{k}, t)\cdot\tilde{\underline{u}}(\underline{k}, t)\rangle\}. \tag{11}$$

Since both $\tilde{\underline{a}}^F(\underline{k}, t)$ and $\tilde{\underline{u}}(\underline{k}, t)$ have zero means, it is evident that $\dot{E}_F$ depends on their correlation. As T_L tends to zero (with σ fixed) this correlation, and hence, $\dot{E}_F$, also tend to zero. However, it is useful to consider the limit as T_L tends to zero with $\epsilon^* \equiv \sigma^2 T_L$ fixed. Then $\tilde{\underline{a}}^F(\underline{k}, t)$ becomes white noise and it can be shown that the rate of energy addition is:

$$\dot{E}_F = 4N_F\epsilon^*. \tag{12}$$

In order that we may consider the non-trivial limit $T_L \to 0$, we take T_L and ϵ^* as the two independent forcing parameters.

SPECIFIED AND CALCULATED QUANTITIES

In this study, we are primarily concerned with three sets of variables, namely, the input parameters, the flow-characterizing variables, and the high-wavenumber quantities. The forcing parameters influence both the flow-characterizing variables (namely, the Reynolds number and the Kolmogorov length-scale) and the high-wavenumber quantities. However, if forcing is to be valid, the input parameters should not influence the latter independently of the former.

The input parameters are: k_0 (the lowest wavenumber), k_{max} (the highest wavenumber), K_F (the maximum wavenumber of the forced modes), ν (the kinematic viscosity), T_L (the forcing time-scale), and ϵ^*. From these quantities four non-dimensional parameters can be formed; we choose these to be $\mathrm{Re}^* \equiv \epsilon^{*1/3}k_0^{-4/3}/\nu$, $T_L^* \equiv T_L\epsilon^{*1/3}k_0^{2/3}$, k_{max}/k_0 and K_F/k_0. The quantity Re* is called the forcing Reynolds number and T_L^* is the nondimensional forcing time-scale. In the present study K_F/k_0 is fixed at either $\sqrt{2}$, or $2\sqrt{2}$; and for 32^3 and 64^3 simulations k_{max}/k_0 is 15.08 and 30.17, respectively.

The three length-scales characterizing the energy-containing scales, the dissipation scales, and the mixed energy-dissipation scales, respectively, are the integral scale:

$$l = \frac{\pi}{2u^2}\int_0^{k_{max}} k^{-1}E(k)\,\mathrm{d}k, \tag{13}$$

the Kolmogorov microscale:

$$\eta = (\nu^3/\epsilon)^{1/4}, \tag{14}$$

and the Taylor microscale:

$$\lambda = \{u^2/\langle(\partial u_1/\partial x_1)^2\rangle\}^{1/2}, \tag{15}$$

where $E(k)$ is the energy spectrum function at the scalar wavenumber $k \equiv (\underline{k}\cdot\underline{k})^{1/2}$, u is the rms value of each component of velocity, and ϵ is the volume-averaged energy-dissipation rate.

The time-scale of the energy-containing eddies is the eddy-turnover time, $T_0 \equiv l/u$. The Reynolds number considered in this study is based on the Taylor microscale, $\mathrm{Re}_\lambda \equiv u\lambda/\nu$. The variables that are most useful in characterizing the simulations are the non-dimensional Kolmogorov length-scale, $k_0\eta$, and the Reynolds number, Re_λ, i.e. simulations which have the same values for these two quantities are expected to be identical, in a statistical sense.

All the forcing parameters have a marked and characteristic effect on the flow-characterizing variables. For simulations with increasing values of Re* (the other non-dimensional input parameters being fixed) the Reynolds number, Re_λ, increases while the non-dimensional Kolmogorov microscale, $k_0\eta$, decreases. Higher values of K_F/k_0 cause a similar effect on the Kolmogorov length-scale by increasing the number of forced nodes and hence the energy-input rate (for fixed Re* and T_L^*), and also significantly reduce the integral length scale. Increased values of T_L^* tend to reduce the energy-input rate (and thereby the steady-state dissipation rate), thus decreasing the Reynolds number and increasing the non-dimensional Kolmogorov microscale, $k_0\eta$.

Among the high-wavenumber quantities considered in the analysis are: the dissipation of dissipation, D_ϵ, and its non-dimensional form, the dissipation skewness, S_ϵ; the variance of the velocity gradient, F_2; and, the velocity-gradient flatness factor, F_4. These quantities tend to depend on the small-scale structure of the velocity field. The dissipation of dissipation and the dissipation skewness are, respectively, defined by:

$$D_\epsilon \equiv 4\nu^2 \int_0^{k_{\max}} k^4 E(k)\,\mathrm{d}k, \tag{16}$$

and

$$S_\epsilon \equiv \tfrac{1}{35}(15/\epsilon)^{3/2}\sqrt{\nu}\,D_\epsilon. \tag{17}$$

(The dissipation of dissipation is so called because, in the balance equation for the mean dissipation rate, it occurs as a destruction term associated with the action of viscosity.) The velocity gradient variance is defined by:

$$F_2 = \langle(\partial u_1/\partial x_1)^2\rangle, \tag{18}$$

and the flatness factor by,

$$F_4 = \langle(\partial u_1/\partial x_1)^4\rangle/F_2^2. \tag{19}$$

These quantities were chosen to give a basis of comparison with Siggia's and Kerr's results.

A list of the input parameters and derived quantities for all the runs is provided in Tables 1 and 2. Table 2 displays, among other quantities, the non-dimensional dissipation, D^*, and the non-dimensional eddy-turnover time, T_0^*, defined by:

$$D^* = \frac{\epsilon}{(3u^2/2)^{3/2}k_0}, \tag{20}$$

and

$$T_0^* = (l/u)(\epsilon^* k_0^2)^{1/3}. \tag{21}$$

NUMERICAL ESTIMATION OF STATISTICAL QUANTITIES

The statistical quantities most commonly used in turbulence analysis are ensemble-averages of instantaneous quantities. As true ensemble-averages cannot be found using direct numerical simulations, time-averages are estimated instead and ergodicity is assumed. These estimated quantities contain statistical errors which must themselves be determined. When appropriate, the statistical quantities are volume-averaged before being time-averaged. This further reduces the extent of the statistical errors.

It is, perhaps, appropriate at this point to provide some indication as to how various quantities were computed. The velocity-gradient variance and the flatness factor were obtained by volume-averaging (in physical space, over all the nodes of the grid) the square

Table 1. Summary of conditions of turbulence simulations: specified quantities

Run	N	C	K_F	ϵ^*	T_L^*	Re*
f1	32	0.796	$2\sqrt{2}$	0.0003	0.0	2.68
f2	"	0.5	"	0.0003	0.0	2.68
f3	"	0.75	"	0.0003	0.0	2.68
f4	"	1.0	"	0.0003	0.0	2.68
f5	"	1.25	"	0.0003	0.0	2.68
f6	"	1.5	"	0.0003	0.0	2.68
f7	"	0.75	"	0.0003	0.0	2.68
f8	"	"	"	0.0008	0.0	3.71
f9	"	"	"	0.0015	0.0	4.58
f10	"	"	"	0.0025	0.0	5.43
f11	"	"	"	0.0035	0.0	6.07
f12	"	"	"	0.0100	0.0	8.62
f13	64	"	"	0.0003	0.0	2.68
f14	"	"	"	0.0008	0.0	3.71
f15	"	"	"	0.0015	0.0	4.58
f17	"	"	"	0.0025	0.0	5.43
f18	"	"	"	0.0035	0.0	6.07
f19	"	"	"	0.0100	0.0	8.62
f21	32	"	"	0.0013	0.100	4.31
f22	"	"	"	0.0019	0.228	4.91
f23	"	"	"	0.0033	0.554	5.96
f24	64	"	"	0.0144	0.078	9.73
f25	"	"	"	0.0220	0.179	11.21
f26	"	"	"	0.0370	0.427	13.33
f27	32	"	$\sqrt{2}$	0.0020	0.0	5.04
f28	"	"	"	0.0033	0.201	5.96
f29	"	"	"	0.0055	0.477	7.06
f30	"	"	"	0.0100	1.164	8.62
f31	64	"	"	0.0350	0.0	13.08
f32	"	"	"	0.0550	0.164	15.21
f33	"	"	"	0.0760	0.360	16.94
f34	"	"	"	0.1350	0.872	20.52
f35	64	"	$2\sqrt{2}$	0.0283	0.0	12.19
f36	32	"	"	0.0283	0.0	12.19

Table 2. Summary of conditions of turbulence simulations: calculated quantities

Run	$k_0\eta$	$k_{max}\eta$	$k_0 l$	Re_λ	S_ϵ	F_4	D^*	T_0^*	ϵ/ϵ^*
f1	0.108	1.64	1.37	16.5	0.635	3.29	0.565	0.191	386.6
f2	0.108	1.64	1.40	17.0	0.628	3.37	0.550	0.192	388.2
f3	0.108	1.64	1.39	16.8	0.631	3.37	0.555	0.193	383.3
f4	0.108	1.64	1.39	16.9	0.630	3.40	0.552	0.192	385.7
f5	0.107	1.61	1.35	16.5	0.640	3.32	0.575	0.188	392.3
f6	0.107	1.61	1.36	16.4	0.780	4.33	0.588	0.188	405.4
f7	0.108	1.64	1.38	16.7	0.632	3.31	0.575	0.193	379.3
f8	0.084	1.24	1.33	22.7	0.577	3.45	0.455	0.172	385.1
f9	0.073	1.09	1.32	27.3	0.547	3.52	0.402	0.165	378.5
f10	0.063	0.95	1.22	29.9	0.522	3.50	0.400	0.151	387.4
f11	0.058	0.87	1.20	32.5	0.501	3.48	0.383	0.147	381.9
f12	0.044	0.66	1.17	42.1	0.440	3.56	0.342	0.136	400.0
f13	0.105	3.17	1.37	17.1	0.626	3.58	0.552	0.184	420.3
f14	0.085	2.56	1.36	23.1	0.584	3.60	0.442	0.176	375.9
f15	0.072	2.17	1.30	27.2	0.566	3.64	0.405	0.162	388.4
f17	0.063	1.90	1.25	30.7	0.552	3.72	0.386	0.153	390.4
f18	0.059	1.78	1.23	33.4	0.548	3.76	0.368	0.153	379.7
f19	0.045	1.36	1.18	42.2	0.529	3.86	0.336	0.138	382.9
f21	0.086	1.30	1.34	21.6	0.592	3.43	0.481	0.211	228.4
f22	0.086	1.30	1.38	22.9	0.585	3.48	0.442	0.238	158.1
f23	0.084	1.27	1.37	23.2	0.575	3.51	0.439	0.281	93.9
f24	0.045	1.36	1.13	40.1	0.531	3.86	0.361	0.154	260.9
f25	0.045	1.36	1.14	41.1	0.527	3.99	0.352	0.176	176.6
f26	0.045	1.36	1.17	41.8	0.524	3.92	0.344	0.211	107.3
f27	0.101	1.52	1.83	29.4	0.541	3.53	0.258	0.338	75.1
f28	0.103	1.55	1.81	28.2	0.537	3.69	0.271	0.409	43.1
f29	0.100	1.51	1.84	31.0	0.531	3.60	0.244	0.453	30.2
f30	0.100	1.51	1.83	30.7	0.528	3.95	0.248	0.549	17.0
f31	0.050	1.50	1.59	53.6	0.513	4.09	0.212	0.279	72.0
f32	0.049	1.48	1.56	54.1	0.508	4.19	0.216	0.311	50.0
f33	0.051	1.54	1.60	53.9	0.517	4.55	0.211	0.368	31.8
f34	0.049	1.48	1.56	53.5	0.512	4.79	0.222	0.418	21.3
f35	0.035	1.06	1.09	51.4	0.505	3.98	0.324	0.127	374.6
f36	0.034	0.51	1.08	49.6	0.359	3.55	0.347	0.126	402.3

and the fourth power of the velocity derivative, respectively. The energy spectrum function, $E(k)$, was computed (for integer k/k_0) by summing the product $\frac{1}{2}\tilde{\underline{u}}(\underline{k}, t)\cdot\tilde{\underline{u}}^*(\underline{k}, t)$ for all $\underline{k}$ such that $k - k_o/2 \leqslant (\underline{k}\cdot\underline{k})^{1/2} < k + k_0/2$. The function thus obtained was smoothed by multiplying it by the ratio of the expected value of the number of nodes in each wavenumber band to the actual number therein. This smoothing is necessary because of the uneven distribution of nodes in the spherical shells forming the wavenumber bands. Numerical integration was used, if needed, to obtain other quantities (e.g. the kinetic energy, S_ϵ, D_ϵ, etc.) that are defined in terms of $E(k)$. The energy-dissipation rate and the Reynolds stresses were computed directly from the Fourier modes of the velocity. It should be mentioned that these quantities, which are computed from summations over the entire spectral space, are automatically volume averaged. The Taylor microscale was computed from the energy and the energy-dissipation rate.

The quantities discussed above are all time-dependent. Their values fluctuate, even after statistical stationarity has been reached by the numerical simulation. They are time-averaged by taking the time-step-weighted mean of the appropriate data. In finding time-averages, the data that pertained to the time-steps before statistical stationarity had been reached was neglected. Based on the findings of the following sections, at least three eddy-turnover time-scales were neglected (by which time statistical stationarity had often been reached). In cases where stationarity was not deemed to have been achieved by this time, greater amounts of data were discarded.

In this study, these statistical errors were estimated by the following means: the autocorrelation functions and the variances of each of the quantities of interest were found, and the variance of the statistical error was computed as $\sigma_{\text{err}}^2 = 2\sigma_q^2 T/T_T$, where T is the integral time-scale (obtained from the appropriate autocorrelation function), T_T is the time-span over which the quantity is averaged, and σ_q is the standard deviation of the quantity under consideration (computed over T_T). For this estimate to be correct, T_T has to be much larger than T (see e.g. Ref. [12]). The square root of the variance of the statistical error is called the standard error. The values of T_T for the simulations presented in Tables 1 and 2 were between 12 and 20 eddy-turnover times. The eddy-turnover time is an indicator of the time-scales of the energy-containing eddies in the flow and is larger than the time-scales of the high-wavenumber quantities. Thus, the condition that T_T should be much greater than T is satisfied in these simulations.

RESULTS

This section consists of the details of a series of numerical tests that used 32^3 and 64^3 flow simulations. The Reynolds number, Re_λ, ranged between 10 and 50, and the Kolmogorov microscale, $k_0\eta$, between 0.035 and 0.11. The 6 components of the volume-averaged Reynolds stress, their dissipation rates, S_ϵ, F_2, F_4, and the dissipation of dissipation, D_ϵ, were saved for each time-step of the computations. From a specified time-step onwards (by which time statistical stationarity was deemed to have been reached) a time-weighted running total of the energy spectrum function at every time-step was kept and was later used to compute the time-averaged function.

All simulations had a randomly specified initial velocity field. This field was generated subject to constraints of isotropy and continuity, and conformed to a specified energy spectrum function [6].

The objectives of the numerical tests to be discussed below were:

(1) To determine when (and if) statistical stationarity is reached.
(2) To determine the effect of the Courant number on the simulations.
(3) To study the effect of the spatial resolution of the grid on the simulations.
(4) To study the effect of the input parameters on flow-characterizing variables, i.e. the Kolmogorov microscale and the Reynolds number.
(5) To study the effect of the forcing time-scale, T_L, on the simulations.
(6) To study the effect of the maximum forcing wavenumber, K_F.

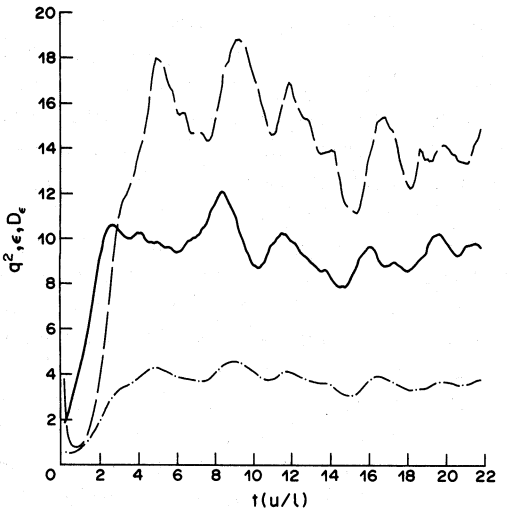

Fig. 1. The evolution of the kinetic energy, energy dissipation, and the dissipation of dissipation for a typical simulation (f24; $k_0\eta = 0.045$). The solid line indicates twice the energy (q^2); the dashed line the dissipation of dissipation; and the lowermost line the energy dissipation. The time is normalized by the eddy-turnover time.

(7) To study the effect of the rectangular grid and the forcing on the isotropy of the velocity field.

1. Stationarity

The velocity fields in the flow simulations take a significant amount of time to reach statistical stationarity. The data from the evolving fields has to be discarded before time-averaging, and hence, it is necessary to know when statistical stationarity is reached. It is, however, impossible to judge precisely if a time-series is statistically stationary unless it is known over very large (technically, infinite) periods. It is also impossible to know definitely when an initially-evolving quantity becomes statistically stationary. In both these matters we have relied on intuitive visual judgement when studying the time-series of the relevant quantities. While this method is subjective, it is probably the best that can be done, and is not a cause for concern.

All the simulations in this study reached approximate statistical stationarity, thereby providing assurance that the forcing scheme performs its primary function satisfactorily. It was observed that the velocity fields take between three to five eddy-turnover times to reach stationarity stationarity.

Figures 1 and 2 show the evolution of the volume-averaged kinetic energy, dissipation, the dissipation of dissipation, the dissipation skewness, and the unnormalized fourth-order derivative correlation, $F_4F_2^2$, as a function of time (in units of eddy-turnover times) for a typical case. In our judgement, the quantities shown have reached statistical stationarity within 5 eddy-turnover times.

Typically, the Reynolds number, S_ϵ, the Kolmogorov microscale, and all the velocity correlations reach steady states from which they deviate only slightly (i.e. fluctuations are generally less than 10% of the mean). In the case of F_4, a highly intermittent quantity, the decision as to when it becomes statistically stationary is a more difficult one. However, stationarity was assumed when the other quantities became approximately so.

2. Courant number

The Courant number, $C\ (= U_{\max}\Delta t/\Delta x)$, is the numerical time-step, Δt, non-dimensionalized by the grid spacing in physical space, Δx, and the maximum velocity. (In Rogallo's code $U_{\max}$ is defined as the maximum, over all the nodes, of the sum of the absolute values of the three velocity components.) It is generally expected in explicit schemes that

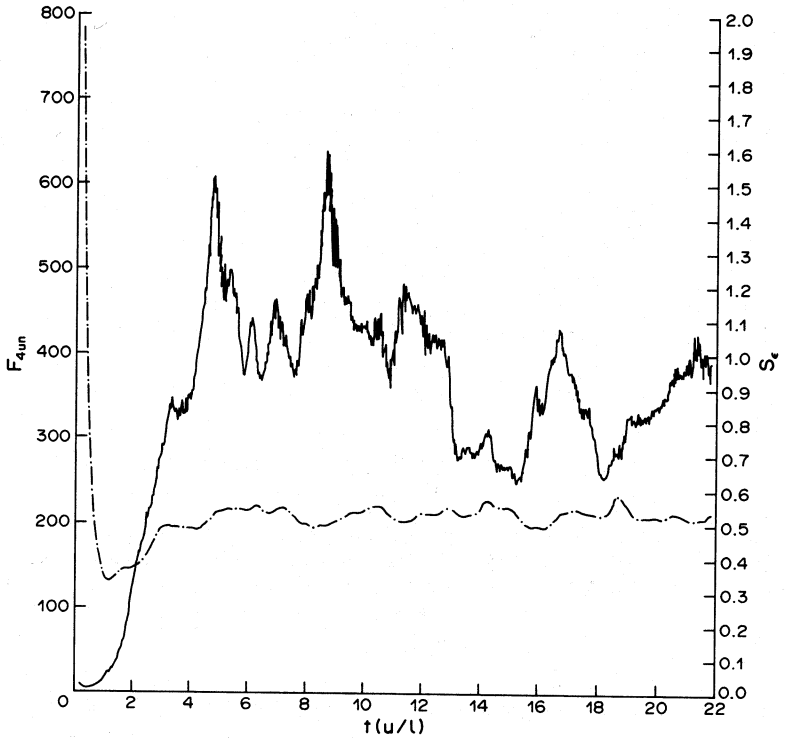

Fig. 2. The evolution of the unnormalized fourth-order velocity-derivative moment (solid line) and the dissipation skewness (dash–dot line) for the same simulation (f24) as in Fig. 1. The time is normalized by the eddy-turnover time.

instabilities can arise when C exceeds a critical value (usually unity). For smaller values of C, the time-stepping errors are generally expected to be proportional to C^2. These considerations suggest the use of a small value of C. But there is a price to pay: the required computer time is inversely proportional to C. Hence one would want to determine the greatest acceptable value of C.

Although Courant number limits for many explicit schemes can be found theoretically, little such work has been done on spectral methods and no such limit is known for the scheme used in Rogallo's code.

In an effort to explore the effect of the Courant number on the simulations, a series of computer runs (f1–f6) were performed for different Courant numbers with the values of the forcing parameters kept fixed. Figure 3 shows the time-averaged values of S_c and F_4. It may be seen that these quantities vary little for $0.5 \leqslant C \leqslant 1.25$ but change dramatically when C is greater than 1.25.

Figure 4 shows the Kolmogorov-scaled energy spectra from the simulations divided by the scaled spectrum obtained from the simulation with the Courant number equal to 0.5. The high-wavenumber end shows considerable deviation from unity (and hence from the more accurate $C = 0.5$ computation) at Courant numbers of 1.25 and above. Similar sets of simulations (with different forcing parameters) also demonstrate such a sharp degradation at critical Courant numbers ranging between 1.0 and 1.25 [16].

Therefore we conclude, along with conventional wisdom, that the Courant number should be chosen close to but not greater than unity. It is, perhaps, worthwhile to emphasize that this Courant number limit arises not because of numerical instability but due to a dramatic falling-off of accuracy.

3. The spatial resolution requirements of the simulations

Good spatial resolution implies that the mesh size of the computational domain is small enough to capture the smallest scales of the turbulence. The smallest scales represented by

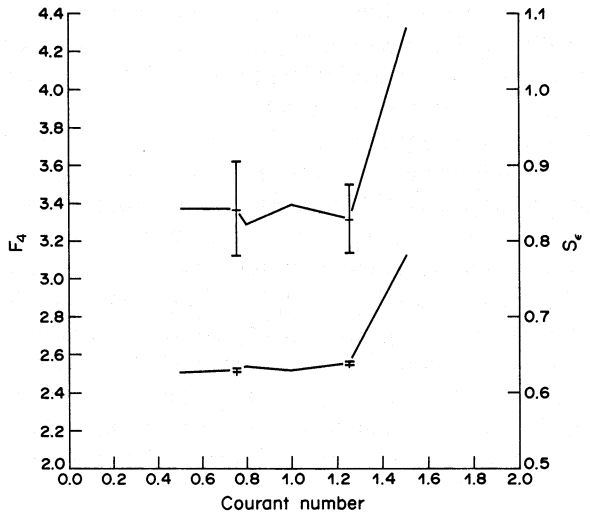

Fig. 3. The fourth-order velocity-derivative moment (upper line) and the dissipation skewness (lower line) are shown against the Courant number for runs f1–6. The error bars are drawn at one standard (statistical) error above and below the mean.

the simulations are of the order of $(1/k_{\max})$ while the smallest turbulent scales are of the order of the Kolmogorov microscale, η. Thus, the non-dimensional quantity $k_{\max}\eta$ has usually been considered the key factor in determining the resolution of the velocity fields. As this quantity decreases the spatial resolution becomes poorer. All other things being equal, the resolution deteriorates as the Reynolds number increases.

In order to be able to judge the quality of a simulation it is important to know the limits of good spatial resolution and the effect of bad resolution. This can be done by comparing the results of 32^3 and 64^3 simulations of identical flows (i.e. with identical input parameter values, except for $k_{\max}/k_0$). The 64^3 grid has a maximum wavenumber twice that of the 32^3

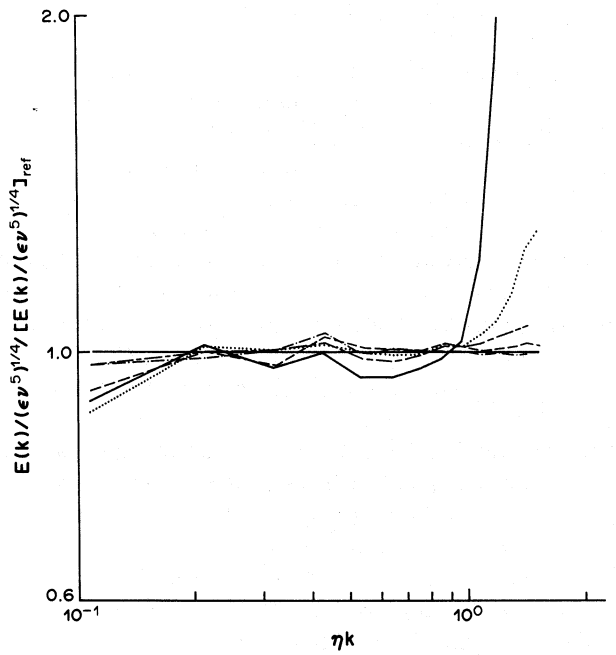

Fig. 4. The Kolmogorov-scaled spectra from simulations (f1–f6) with various Courant numbers divided by the Kolmogorov-scaled spectrum from a simulation with $C = 0.5$. Lines: (—·—) $C = 0.75$; (———) $C = 0.80$; (—·—) $C = 1.0$; (· · · ·) $C = 1.25$; (———) $C = 1.5$.

grid and therefore has twice the resolution. Comparison of twin sets of such simulations shows that the results diverge from each other for simulations with decreasing values of $k_{\max}\eta$. This is caused by the degradation of the quality of the 32^3 simulations (assuming that the 64^3 simulations are relatively accurate).

Figures 5 and 6 show time-averaged values of S_c and F_4 for 32^3 and 64^3 simulations over a range of Kolmogorov length-scales. The skewness values diverge slowly with decreasing values of $k_{\max}\eta$ until the latter quantity reaches a value around unity, below which the divergence is much more rapid. A similar trend may exist for F_4 (Fig. 6), but the statistical errors in this case are too large to allow a definite conclusion. Figures 7–10 display the Kolmogorov-scaled dissipation spectra for some of the same simulations. The figures demonstrate the same trend as Fig. 5, i.e. slow degradation of the simulations until $k_{\max}\eta$ reaches a value of about 0.9, followed by relatively rapid degradation for lower values.

These results indicate that a value of $k_{\max}\eta$ of about 1.0 is near the limit of good resolution. Quantities that are dominated by the extreme high-wavenumber end of the energy spectrum, however, may have more stringent requirements (see Ref. [11]).

4. *The parametrization of the Kolmogorov length-scale and the Reynolds number*

Simulated flows are generally characterized by the non-dimensional Kolmogorov microscale, $k_0\eta$, and Reynolds number, Re_λ. It is useful, therefore, to be able to choose the values of the forcing parameters that yield simulations with a prescribed $k_0\eta$ and Re_λ without having to resort to guesswork. This means that these quantities have to be parametrized in terms of T_L^*, the forcing time-scale, Re*, the forcing Reynolds number, and N_F, the number of nodes in the forced wavenumber band (or alternately, K_F, the maximum forced wavenumber), all of which play important roles in determining the flow variables.

We have developed a simple model which describes the dependence of $k_0\eta$ on the forcing parameters quite well.

Consider $\tilde{u}_i(\underline{k}, t)$, the Fourier component of velocity at discrete wavenumber $\underline{k}$. If in eqn (7), we model $\tilde{a}_i(\underline{k}, t)$, by $-\tilde{u}_i(\underline{k}, t)/T_e$, where T_e is a time-scale (as yet undefined), we obtain:

$$\frac{\partial \tilde{u}_i(\underline{k}, t)}{\partial t} = -\frac{\tilde{u}_i(\underline{k}, t)}{T_e} + \tilde{a}_i^F(\underline{k}, t). \tag{22}$$

Then, from eqn (22) we obtain:

$$\frac{\partial \frac{1}{2}\langle \tilde{u}_i(\underline{k}, t)\tilde{u}_i^*(\underline{k}, t)\rangle}{\partial t} = -\frac{\langle \tilde{u}_i(\underline{k}, t)\tilde{u}_i^*(\underline{k}, t)\rangle}{T_e} + \tfrac{1}{2}\langle \tilde{u}_i^*(\underline{k}, t)\tilde{a}_i^F(\underline{k}, t)\rangle + \tfrac{1}{2}\langle \tilde{u}_i(\underline{k}, t)\tilde{a}_i^{F*}(\underline{k}, t)\rangle. \tag{23}$$

In the statistically stationary state, the term on the left-hand side of eqn (23) vanishes, and we can readily identify the first term on the right-hand side as the energy taken out of the Fourier component under consideration, and it follows that the dissipation, ϵ, is given by:

$$\epsilon = \frac{1}{2}\sum_{m_1}\sum_{m_2}\sum_{m_3}\{\langle \tilde{u}_i^*(\underline{k}, t)\tilde{a}_i^F(\underline{k}, t)\rangle + \langle \tilde{u}_i(\underline{k}, t)\tilde{a}_i^{F*}(\underline{k}, t)\rangle\}. \tag{24}$$

Knowing that $a_i^F(\underline{k}, t)$ is defined by Uhlenbeck–Ornstein processes as described above, and using eqn (22), we can analytically derive the expected value $\langle u_i^*(\underline{k}, t)\tilde{a}_i^F(\underline{k}, t)\rangle$ to obtain:

$$\epsilon = \frac{4\epsilon^* T_e N_F}{T_L + T_e}. \tag{25}$$

In the expression on the right-hand-side of eqn (25) only the quantity T_e is not directly defined in terms of the input parameters. In an attempt to predict the energy-dissipation rate we replace T_e by the estimate $\beta/(N_F\epsilon^* k_0^2)^{1/3}$, where β is a constant. This guess, that can be fully justified only *a posteriori*, is based on the assumptions that ϵ scales (roughly) with $N_F\epsilon^*$, and that the integral length scale scales with k_0^{-1}. With this estimate for T_e,

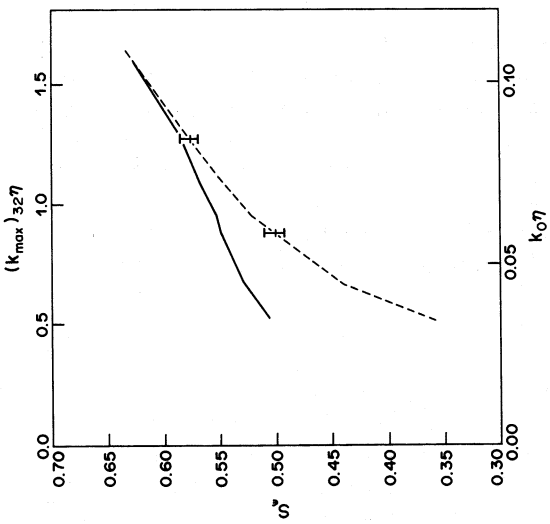

Fig. 5. Effect of spatial resolution on the dissipation skewness. S_ϵ against Kolmogorov length-scale for 64^3 simulations (solid line, f13–19, f36) and for 32^3 simulations (dashed line, f7–12, f35). The corresponding values of $k_{max}\eta$ for the 32^3 simulations are shown at the top. The error bar shows one standard (statistical) error above and below the mean.

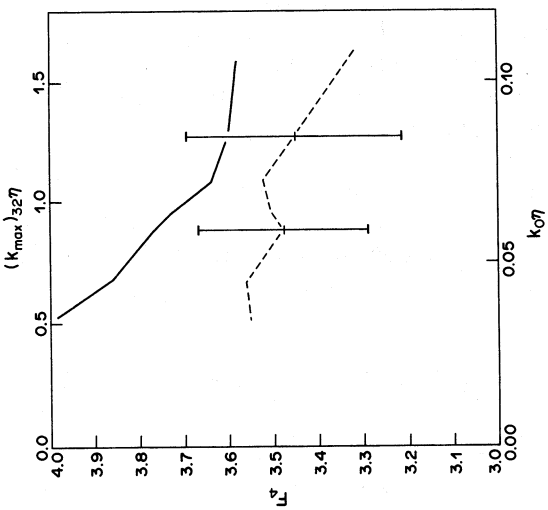

Fig. 6. Same as Fig. 5 but displays the fourth-order velocity derivative moment.

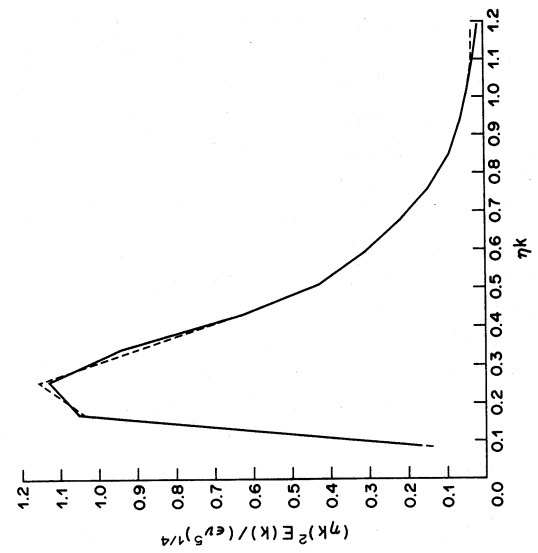

Fig. 7. The effect of spatial resolution on the computed dissipation spectrum: Kolmogorov scaled spectrum for a 64^3 simulation (f14, $k_{max}\eta = 2.56$, solid line) and a 32^3 simulation (f8, $k_{max}\eta = 1.24$, dashed line) with identical forcing parameters.

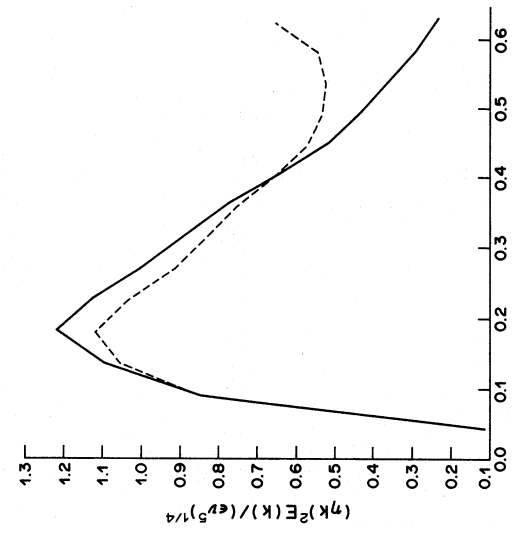

Fig. 10. The same as Fig. 7 except: solid line 64^3 simulation (f19, $k_{\max}\eta = 1.36$); Dashed line 32^3 simulation (f12, $k_{\max}\eta = 0.66$).

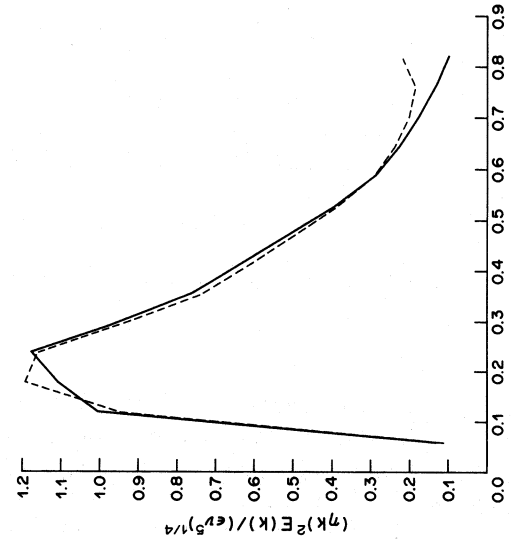

Fig. 9. The same as Fig. 7 except: solid line 64^3 simulation (f18, $k_{\max}\eta = 1.78$); Dashed line 32^3 simulation (f11, $k_{\max}\eta = 0.87$).

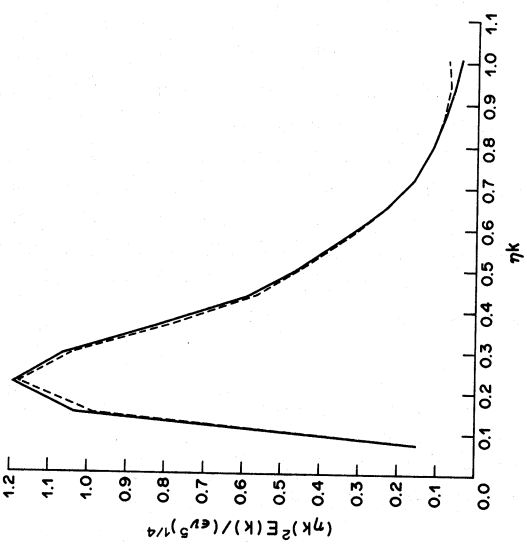

Fig. 8. The same as Fig. 7 except: solid line 64^3 simulation (f15, $k_{\max}\eta = 2.17$); Dashed line 32^3 simulation (f9, $k_{\max}\eta = 1.09$).

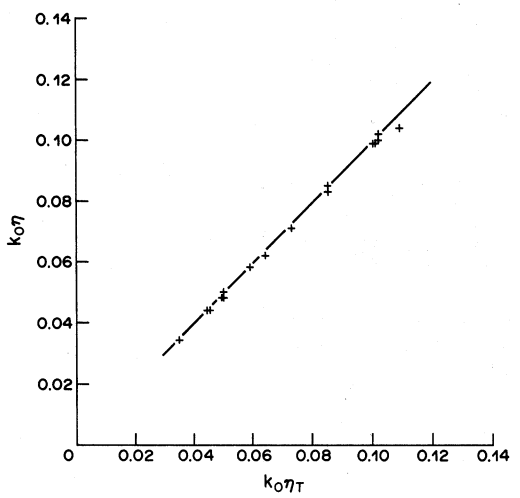

Fig. 11. The non-dimensional Kolmogorov length-scale (from simulations f13–35) against the parameter $k_0\eta_T$.

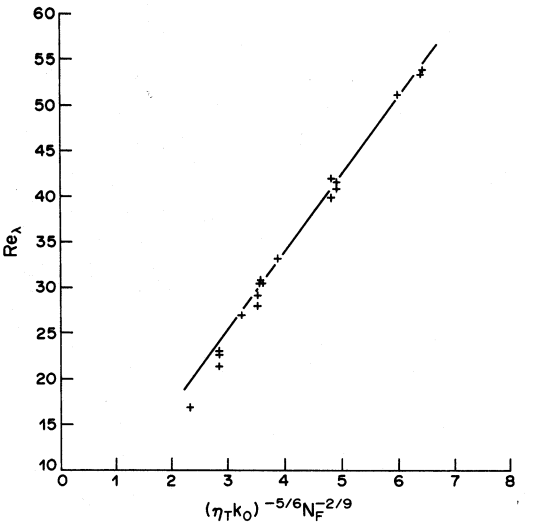

Fig. 12. The Reynolds number (from simulations f13–35) against the parameter $(\eta_T k_0)^{-5/6} N_F^{-2/9}$. The solid line indicates $8.5/(\eta_T k_0)^{5/6} N_F^{2/9}$.

eqn (25) becomes:

$$\epsilon_T^* \equiv \frac{4\epsilon^* N_F}{1 + T_L^*(N_F)^{1/3}/\beta}, \tag{26}$$

where ϵ_T^* is the predicted value of the energy-dissipation, ϵ. The quantity that predicts the Kolmogorov microscale is,

$$\eta_T \equiv (\nu^3/\epsilon_T^*)^{1/4}. \tag{27}$$

Figure 11 shows the non-dimensional Kolmogorov microscale, $k_0\eta$, vs $k_0\eta_T$ (with $\beta = 0.8$) for the well-resolved simulations. The data points from the various simulations fall on or very close to the line $k_0\eta = k_0\eta_T$, thereby demonstrating that η_T accurately predicts the value of the Kolmogorov microscale to be obtained from a simulation.

The Reynolds number was found to be represented reasonably well by the empirical expression:

$$Re_\lambda \approx \frac{8.5}{(\eta_T k_0)^{5/6} N_F^{2/9}}. \tag{28}$$

This curve is displayed in Fig. 12 along with the simulation data points.

It should be mentioned that only two values of K_F, i.e. $\sqrt{2}k_0$ and $2\sqrt{2}k_0$, with corresponding values of N_F of 18 and 92, respectively, were used in the simulations in this study. Hence the power-law dependencies of N_F in eqns (26) and (28) are tentative.

In order to find the values of ϵ^*, T_L^*, ν and N_F, that yield prescribed values of Re_λ, and $k_0\eta$ in a simulation, the following procedure can be used: First, after arbitrarily choosing ν, ϵ_T^* and N_F can be obtained from eqns (27) and (28). Then, knowing ϵ_T^*, and choosing a value for T_L^*, ϵ^* can be found by using eqn (26).

5. The effect of the forcing time-scale T_L^*

In order to show that the high-wavenumber quantities are not directly affected by the choice of forcing parameters one would have to demonstrate that simulations with different sets of forcing parameters but with the same Reynolds number and Kolmogorov microscale yield essentially the same values for the time-averaged high-wavenumber quantities.

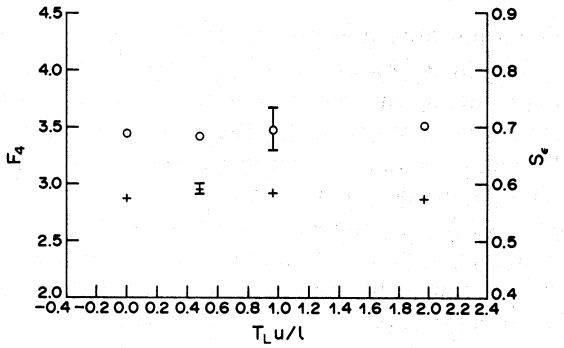

Fig. 13. Effect of forcing time-scale on small-scale statistics. Fourth-order velocity derivative moment (circles) and dissipation skewness (pluses) against the normalized forcing time scale. From 32^3 simulations f8, f21–23, $\mathrm{Re}_\lambda \approx 22$, $K_F = 2\sqrt{2k_0}$.

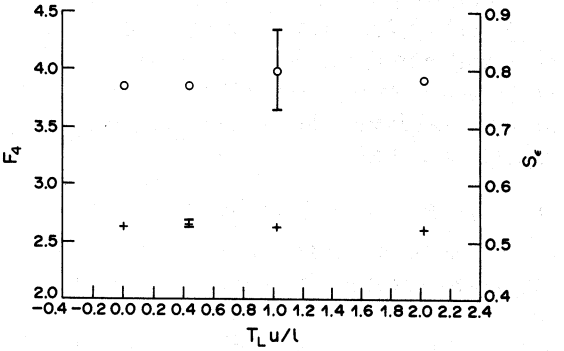

Fig. 14. The same as Fig. 13 but with 64^3 simulations, f19, f24–26; $\mathrm{Re}_\lambda \approx 41$, $K_F = 2\sqrt{k_0}$.

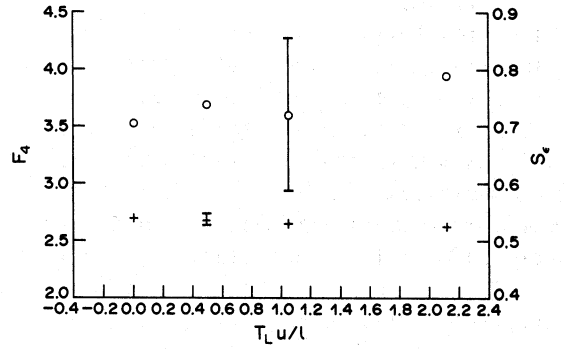

Fig. 15. The same as Fig. 13 but with 32^3 simulations f27–30; $\mathrm{Re}_\lambda \approx 30$, $K_F = \sqrt{2k_0}$.

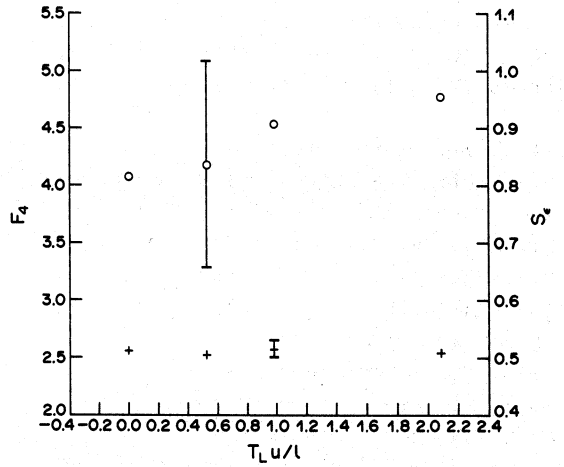

Fig. 16. The same as Fig. 13 but with 64^3 simulations f31–34; $\mathrm{Re}_\lambda \approx 54$, $K_F = \sqrt{2k_0}$.

In order to test this proposition, four sets of simulations were performed: 32^3 and 64^3 simulations for two values of K_F/k_0, $\sqrt{2}$ and $2\sqrt{2}$, respectively. Each set consisted of 4 simulations in which the forcing time-scale, T_L, ranged from 0 to 2 eddy-turnover times. The other forcing parameters were chosen (by the procedure outlined in the last section) such that the Reynolds number and the Kolmogorov microscale were kept approximately constant for all the simulations in any one set.

The dissipation skewness, S_ϵ, and the fourth-order derivative moment, F_4, for the four sets of simulations are shown in Figs 13–16. The values corresponding to the simulations in each set demonstrate a remarkable consistency and the differences between them fall well within the statistical error bars.

Figures 17–20 show the Kolmogorov-scaled dissipation spectra for the same simulations. Once again, the high-wavenumber regions of the spectra in any set show great uniformity and are often barely distinguishable from each other.

As these sets of simulations cover a range of forcing parameters, grid sizes, and Reynolds numbers, the results outlined above seem to provide powerful evidence that, for any given Reynolds number and non-dimensional Kolmogorov microscale, the values of high-wavenumber quantities can be expected to be independent of the choice of forcing parameters. This justifies the validity of the use of forced direct numerical simulations in studies of high-wavenumber quantities.

6. The effect of the maximum forcing wavenumber, K_F

All the simulations in this study used either one of two values of K_F, i.e. $\sqrt{2}k_0$ or $2\sqrt{2}k_0$. The differences between these respective simulations shed some light on the nature of the flow-characterizing variables.

The choice of K_F has a marked effect on the integral length-scale of the velocity field. Smaller values of K_F result in higher values of the integral length-scale. The Reynolds number values for simulations with different values of K_F, but with the same value of the non-dimensional Kolmogorov length-scale, are quite different. The energy spectrum functions from two such simulations are also quite different from each other in the low-wavenumber range, even when they are scaled by the large-scale quantities u and l. This can be seen, for example, in the energy spectrum functions from two simulations with approximately the same Kolmogorov length-scale, but different K_F shown in Fig. 21. This leads one to the to-be-expected conclusion that the two flow-simulations are, in fact, quite dissimilar. This is also the case when similar comparisons are made of simulations with the same Reynolds number but different values of the Kolmogorov length-scale (for two distinct values of K_F).

In the analysis of high-Reynolds-number flows, in turbulence research, it is generally deemed sufficient to treat the Reynolds number, Re_λ, alone as the flow-characterizing variable. This is because high-wavenumber quantities are presumed to be functionally dependent primarily on the energy-dissipation, viscosity, and the wavenumber, and the effect of the large scales is thought to be relatively weak and dependent (at least to a first approximation) on the Reynolds number. This idea derives from Kolmogorov's refined hypotheses [17].

It is true, in the simulations studied, that there exists a region in the energy spectrum that is mainly influenced by the energy-dissipation and the viscosity and is universal when scaled by Kolmogorov variables (i.e. showing no Reynolds-number-dependence in the range under consideration). This may be seen in the Kolmogorov-scaled dissipation functions (taken from simulations with quite disparate values for the Reynolds number, the Kolmogorov length-scale and the integral length-scale) displayed in Fig. 22: they are nearly identical in the high-wavenumber end.

However, a study of the high-wavenumber quantities in Table 1 and 2 shows that they are not exclusively dependent on either the Reynolds number or the non-dimensional Kolmogorov length-scale. Thus, it has become apparent that forced turbulent simulations have to be characterized by, at least, the Reynolds number Re_λ, and the non-dimensional Kolmogorov length-scale, $k_0\eta$. It can be argued, however, that these two quantities are

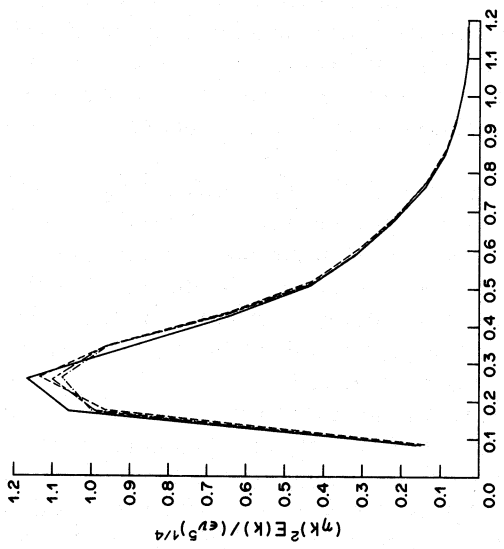

Fig. 17. The effect of forcing time-scale on the dissipation spectrum: the Kolmogorov-scaled dissipation spectrum is shown for various values of the non-dimensional forcing time-scale ($T_L u/l$). From 32^3 simulations f8, f21–23, $Re_\lambda \approx 22$, $K_F = \sqrt{2}k_0$. (——) ($T_L u/l = $) 0; (——) 0.48; (—·—) 0.96; (—··—) 1.97.

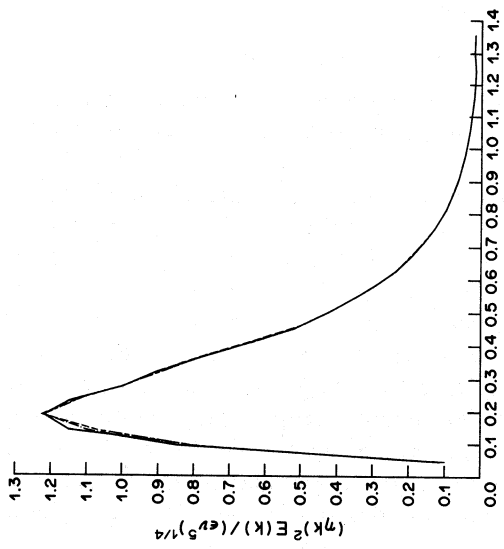

Fig. 18. The same as Fig. 17 but for 64^3 simulations f19, f24–26; $Re_\lambda \approx 41$, $K_F = 2\sqrt{2}k_0$. (——) ($T_L u/l = $) 0; (——) 0.43; (—·—) 1.02; (—··—) 2.02.

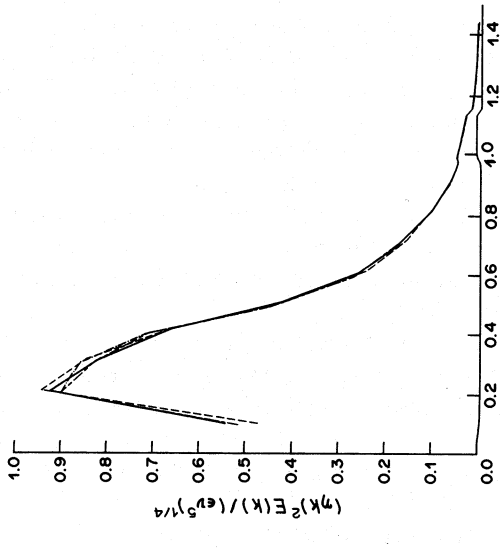

Fig. 19. The same as Fig. 17 but for 32^3 simulations f27–30; $Re_\lambda \approx 30$, $K_F = \sqrt{2}k_0$. (——) ($T_L u/l = $) 0; (——) 0.49; (—·—) 1.05; (—··—) 2.12.

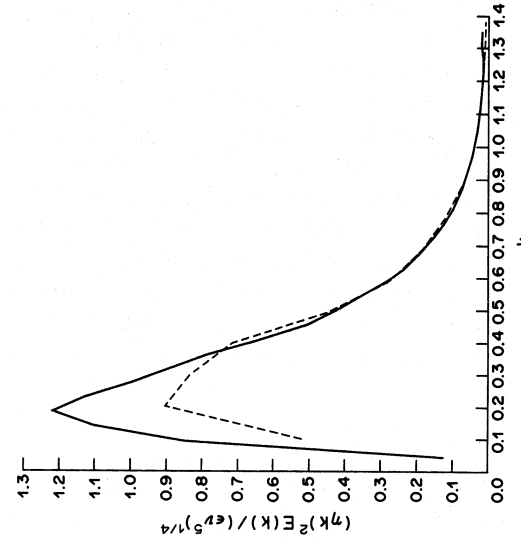

Fig. 22. The invariance of the high-wavenumber region of the Kolmogorov-scaled dissipation spectrum is demonstrated. Data from simulations f19 (solid line) ($Re_\lambda = 42.2$ $k_0\eta = 0.045$; $K_F/k_0 = 2\sqrt{2}$; $lk_0 = 1.18$) and f30 ($Re_\lambda = 30.7$; $k_0\eta = 0.100$; $K_F/k_0 = \sqrt{2}$; $l = 1.83$).

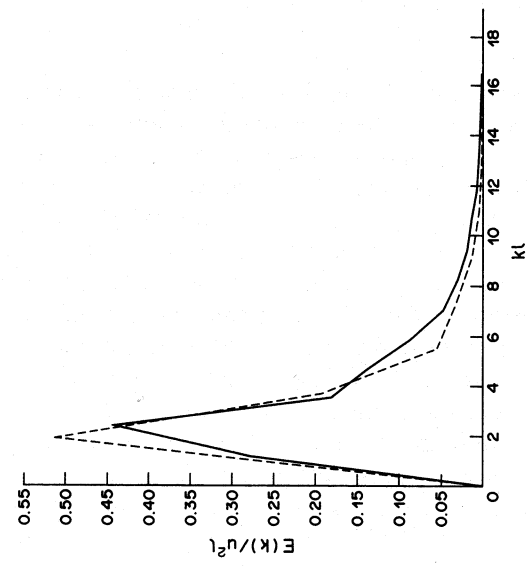

Fig. 21. The effect of the maximum forcing wavenumber on the energy spectrum. The energy spectrum is shown against the wavenumber (both are non-dimensionalized by large-scale quantities) for 64^3 simulations, f19 (solid line) ($Re_\lambda = 42.2$; $k_0\eta = 0.045$; $K_F/k_0 = 2\sqrt{2}$) and f31 ($Re_\lambda = 53.6$; $k_0\eta = 0.05$; $K_F/k_0 = \sqrt{2}$).

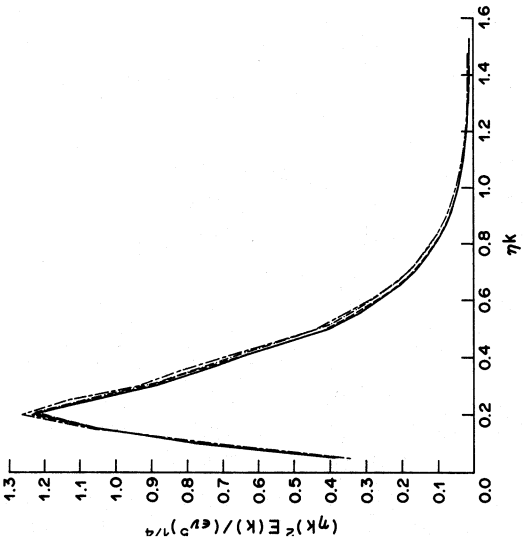

Fig. 20. The same as Fig. 17 but for 64^3 simulations f31–34; $Re_\lambda \approx 54$, $K_F = \sqrt{2}k_0$. (——) $(T_L u/l =)$ 0; (— — —) 0.53; (— · —) 0.98; (— · · —) 2.08.

sufficient to characterize the flow simulations: it is already known that the parameters Re*, T_L^*, K_F/k_0, and k_{max}/k_0 are sufficient to characterize statistically-stationary simulations. Of these, k_{max}/k_0 is of little importance if the simulation is well-resolved. It is reasonable to assume that, given Re* and T_L^*, K_F/k_0 has a one-to-one relationship with the pair-combination comprising of the Reynolds number, Re_λ, and the non-dimensional Kolmogorov length-scale, $k_0\eta$ (as the latter quantity is a monotonic function of K_F/k_0, other non-dimensional input parameters being fixed). Therefore, Re*, T_L^*, Re_λ, and $k_0\eta$ are sufficient to describe the simulations. However, there is considerable evidence to show that combinations of Re* and T_L^* which yield the same values of Re_λ and $k_0\eta$ also produce the same values for all other derived quantities (both high-wavenumber and large-scale) in the simulations. Thus, Re_λ and $k_0\eta$ can be chosen as the two independent quantities sufficient (and necessary) to characterize the flow (at least for the 32^3 and 64^3 simulations in this study).

7. *Anisotropy in the velocity fields*

DNS are performed on a cubical grid. Such a grid is inherently anisotropic, and consequently, so is the forcing that is being done on it. To determine if this causes the velocity field to deviate significantly from isotropy, we computed the correlation function $R_{33}(x_1, x_2, x_3)$ $(\equiv \langle u_3(y_1, y_2, y_3)u_3(y_1 + x_1, y_2 + x_2, y_3 + x_3)\rangle / \langle u_3^2 \rangle)$. For a homogeneous, isotropic field, this function has circular contours in the $x_1 - x_2$ plane, i.e. it will depend only on $r \equiv (x_1^2 + x_2^2)^{1/2}$.

The simulations in this study have no preferential choice, in a statistical sense, for any of the directions along the axes of the computational grid. Therefore anisotropy will exhibit itself in $R_{33}(x_1, x_2, x_3)$ only when values of that function are contrasted for spatial separations (r) along axial and non-axial directions.

Figures 23–24 contrasts $R_{33}(r, 0, 0)$ (the "axial" correlation) with $R_{33}(r/\sqrt{2}, r/\sqrt{2}, 0)$ (the "diagonal" correlation) for two typical simulations. (These two functions were computed from the appropriate time-averaged component of the energy spectrum function tensor, i.e. $E_{33}(k_1, k_2, 0)$.) Because of the obvious symmetry, only one-half (i.e. $r \geqslant 0$) of the function space is shown. In both cases, the "axial" and "diagonal" functions are very close together (except for large r). The difference between the two at large values of r is not unexpected given their different periodicities. (The "axial" correlation function has a period of N grid spacings while the "diagonal" function's period is $\sqrt{2}N$.)

The difference between the two functions is so much less than the expected statistical error that, perhaps, an explanation is in order. This occurs because the "axial" and

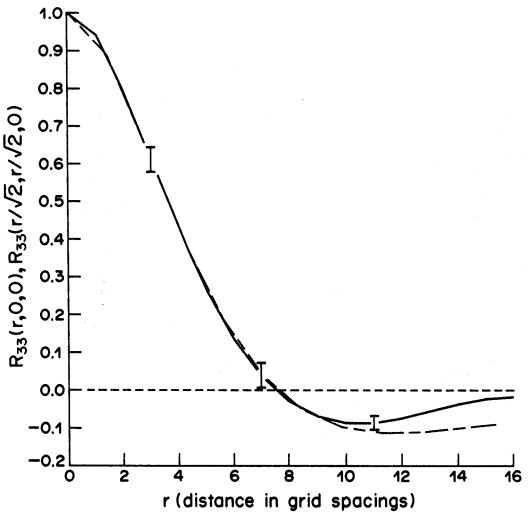

Fig. 23. The effect of forcing on the isotropy of the correlation function, $R_{33}(x_1, x_2, x_3)$. The solid line indicates $R_{33}(r, 0, 0)$, and the dashed line $R_{33}(r/\sqrt{2}, r/\sqrt{2}, 0)$. (From 32^3 simulation f9.)

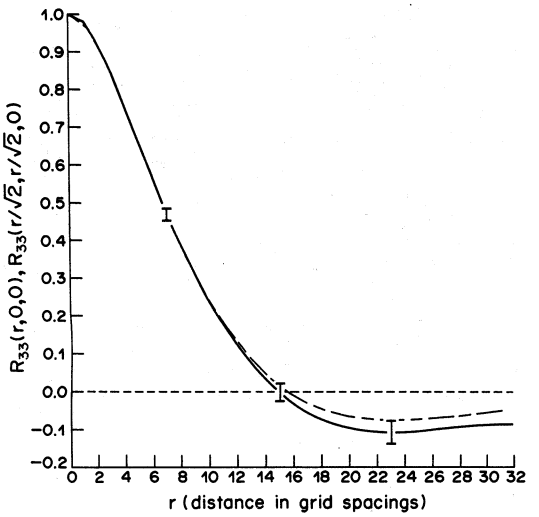

Fig. 24. The same as Fig. 23 but for 64^3 simulation f17.

"diagonal" correlation functions are not independent of each other and as they are computed from the same simulation they may thus be expected to be correlated with each other.

No simple test such as this can prove isotropy—but that the results above definitely suggest that gross anisotropy is absent.

CONCLUSION

The use of spectral forcing to obtain statistically stationary velocity fields in direct numerical simulations of homogeneous, isotropic flows has been tested and validated. The limits imposed on the non-dimensional time-step, the Courant number, by the need for good quality numerical simulations, and also the spatial resolution requirements of the latter have been studied and quantified.

The results of this study are summarized below:

A forcing scheme has been developed to provide a means of obtaining statistically stationary simulations of homogeneous, isotropic turbulence. The scheme involves the addition of energy to the Fourier modes of velocity at wavenumbers inside a low-wavenumber shell. This additional energy is obtained from a formulation based on Uhlenbeck–Ornstein random processes. The forcing scheme works well, and the forced simulations yield statistically stationary velocity fields that display no gross anisotropy nor unreasonably high correlation times.

The effect of the forcing scheme on high-wavenumber-dependent quantities of the velocity fields has been explored. Over a number of test-cases, the values of the high-wavenumber quantities obtained from simulations with the same Reynolds number and Kolmogorov length-scale, but with different sets of forcing parameters, deviated from each other by no more than the expected statistical error. This shows that the details of the forcing do not have an undue influence on the values of the high-wavenumber quantities.

The Courant number has a marked effect on the flow-simulations when it exceeds a critical value. The values of the high-wavenumber quantities obtained from simulations with the Courant number greater than about 1.0–1.25 deviated significantly from those obtained from simulations with lower Courant number values. A Courant number value of unity essentially defines the acceptable upper limit, if one is to avoid significant time-stepping errors.

The spatial resolution of the velocity fields by the computational grid is dictated by the value of the parameter $k_{max}\eta$, where k_{max} is the maximum significant wavenumber in

the simulation, and η is the Kolmogorov length-scale. We found that the quality of the simulations deteriorates significantly when this parameter is below unity.

It was our intention in this study, among other things, to validate the use of our spectral forcing scheme. This forcing scheme is to be used to obtain statistically stationary turbulent flow-simulations for the purpose of studying the small-scale behavior of such flows. However, in 32^3 and even in 64^3 simulations, the range of the length-scales that can be considered small compared to the integral length-scale is quite limited. Studies of the small-scale structure of turbulent flows will be better served by simulations on larger computational grids. We intend to steer such a course in the future.

Acknowledgements—We are grateful to Dr R. S. Rogallo for providing us with the computer code, and for his patient advice on its use.

This work was supported in part by the Cornell Center of Theory and Simulation and in part by the U.S. Air-Force Office of Scientific Research (grant number AFOSR-85-0083). Computations conducted during the research were performed at the Cornell National Supercomputer Facility, which is supported in part by the National Science Foundation, New York State, and the IBM Corporation.

REFERENCES

1. R. S. Rogallo and P. Moin, Numerical simulations of turbulent flows. *Ann. Rev. Fluid Mech.* **16,** 99 (1984).
2. E. D. Siggia and G. S. Patterson, Intermittency effects in a numerical simulation of stationary three-dimensional turbulence. *J. Fluid Mech.* **86,** 567 (1978).
3. E. D. Siggia, Numerical study of small-scale intermittency in three-dimensional turbulence. *J. Fluid Mech.* **107,** 375 (1981).
4. R. M. Kerr, Higher-order derivative correlations and the alignment of small-scale structures in isotropic numerical turbulence. *J. Fluid Mech.* **153,** 31 (1985).
5. S. A. Orszag and G. S. Patterson, Numerical simulation of turbulence. *Statistical Models and Turbulence, Lecture Notes in Physics*, Vol. 12. Springer, New York (1972).
6. R. S. Rogallo, Numerical experiments in homogeneous turbulence. NASA TM-81315 (1981).
7. R. W. Metcalfe and J. J. Riley, Direct Numerical Simulations of turbulent shear flows. Proc. Int., Conf. Numer. Methods Fluid Dyn., 7th, Stanford-Ames (1980); *Lecture Notes in Physics*, Vol. 141. Springer, New York (1981).
8. D. Gottlieb and S. A. Orszag, Numerical analysis of spectral methods: theory and application. *CBMS-NSF Reg. Conf. Ser. Appl. Math.* Vol. 26. SIAM, Philadelphia (1977).
9. N. N. Mansour, P. Moin, W. C. Reynolds and J. H. Ferziger, Improved methods for large eddy simulations of turbulence. *Turbulent Shear Flows* Vol. I, p. 386. Springer, New York (1979).
10. M. Y. Hussaini and T. A. Zang, Spectral methods in Fluid Mechanics. *Ann. Rev. Fluid Mech.* **19,** 339 (1987).
11. P. K. Yeung and S. B. Pope, An algorithm for tracking fluid particles in numerical simulations of homogeneous turbulence. *J. Comput. Phys.* (In press).
12. H. Tennekes and J. L. Lumley, *A First Course in Turbulence.* MIT Press, Cambridge (1972).
13. A. N. Kolmogorov, Local structure of turbulence in an incompressible fluid at very high Reynolds numbers. *C. R. Acad. Sci. USSR* **30,** 301 (1941).
14. R. Peyret and T. D. Taylor, *Computational Methods for Fluid Flow.* Springer, New York (1983).
15. N. Wax, *Selected papers on Noise and Stochastic Processes.* Dover, New York (1954).
16. V. Eswaran, An examination of forcing in Full Turbulence Simulations. Tenth Symposium on Turbulence, Missouri-Rolla (1986).
17. A. N. Kolmogorov, A refinement of previous hypotheses concerning the local structure of turbulence in a viscous incompressible fluid at high Reynolds number. *J. Fluid Mech.* **13,** 82 (1962).